PHYSICAL REVIEW A VOLUME 8, NUMBER 4 OCTOBER 1973

Heavy-Ion-Induced X-Ray Production in Solids

K. Taulbjerg, B. Fastrup, and E. Laegsgaard
Institute of Physics, University of Aarhus, DK 8000 Aarhus, Denmark
(Received 2 April 1973)

The Fano-Lichten model is known to be in good accord with available inner-shell excitation data on gaseous targets, whereas there exist several examples of discrepancies between the model and results of solid-target experiments. As will be discussed in detail in this paper, these apparent discrepancies may be explained by so-called "solid effects." An equation taking due account of energy-loss straggling, x-ray generation in recoil collisions, and targets absorption of emitted x rays is used to relate the measured x-ray yield to an x-ray production cross section averaged over the equilibrium distribution of projectile charge states in the solid. Experimental cross sections are reported for the Al K x-ray production in Al targets bombarded with N, Al, and Ar ions, and for the Ne K x-ray production of Ne projectiles incident on Mg, Al, Si, and P targets. The neglect of solid effects in published x-ray data is commented upon.

I. INTRODUCTION

During recent years there has been a rapidly increasing interest in the study of violent heavy-ion–atom collisions at relative nuclear velocities small compared to the orbital velocities of inner-shell electrons in the colliding particles. Such collisions, which can be very efficient in producing inner-shell vacancies (see, e.g., Ref. 1), have been investigated by inelastic-energy-loss measurements, Auger electron spectroscopy, and x-ray spectroscopy. Since these methods are more or less complementary, none of them is able to provide a complete insight into the collision process. To establish an understanding of the excitation and de-excitation mechanisms, it is therefore very useful to have available a broad variety of experimental data, obtained from all three methods.

The interpretation of the experimental data is based on the Fano-Lichten[2,3] or the molecular-orbital (MO) model. In this model it is assumed that owing to the small relative nuclear velocity of the colliding particles, inner-shell electrons may adjust their orbital motion quasiadiabatically to the slowly varying two-center field, such that molecularlike electron states (MO), depending parametrically on the internuclear separation distance R, are formed. If, during the collision, two MOs become degenerate or almost degenerate at a definite value of R, a strong dynamic coupling, caused by the nuclear motion may result. Such dynamic couplings call for a change in the description of the colliding system. Instead of using static, adiabatic MOs, it is more convenient to use dynamic diabatic states[2-4] which, unlike the adiabatic states, do not obey the noncrossing rule. A diabatic MO may correlate an atomic state of the separated atoms with an atomic state of the united atom whose principal quantum numbers differ appreciably (promotion). If so, the diabatic MO crosses other MOs as R is varied during the collision, and one or more electrons may be transferred from their initial state to an excited state, and when the atoms have separated, one or more inner-shell vacancies have been produced. In lack of precise MO energy-level diagrams, simple diabatic-correlation diagrams have been useful in the interpretation of inelastic collisions. For the construction of such diagrams, see Ref. 3. Figure 1 shows a simple diabatic correlation diagram representing the system under discussion.

In recent years, several experiments have been devoted to the determination of x-ray yields versus energy in ion-solid collisions. Although such data are relatively easy to obtain, their interpretation in terms of inner-shell excitation cross sections is a tricky problem. First of all, lack of precise information of the fluorescence yields for the different subshells in the ionic collision products makes, even for gaseous targets, an evaluation of the ionization cross sections from measured x-ray yields rather uncertain. Second, the use of thick targets both to achieve higher x-ray intensities and to increase the number of accessible target elements gives rise to so-called "solid effects."

The charge state of the ions traversing the solid is repeatedly changed by capture and loss processes, such that the precollision state of the projectile is unspecified and changes from one collision to another. An equilibrium charge-state distribution of the projectiles is obtained after they have penetrated a few atomic layers below the surface of the solid target, and consequently, the projectile ions lose memory of their initial charge state. Since it is known from both inelastic-energy-loss measurements[5] and Auger-elec-

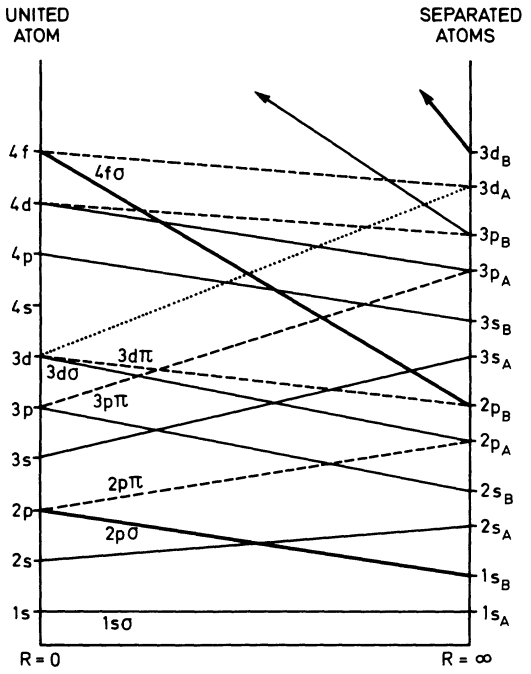

FIG. 1. Diabatic MO correlation diagram for the case of Z_A slightly larger than Z_B. Solid lines correspond to σ states, dashed lines to π states, and dotted lines to δ states.

tron measurements[6] that the probability for producing an inner-shell vacancy in some cases depends strongly on the precollision charge state of the particles, it follows that ion-solid interactions may become very difficult to analyze rigorously.

Another solid effect is due to the creation of recoils in the solid target. Such recoils, which may have a considerable kinetic energy, will in collisions with other atoms produce additional inner-shell ionizations in target atoms.[7]

Although studies of x-ray production in solids require a complicated data analysis and, as will be discussed later, the evaluated production cross sections represent averages of more specific cross sections, these studies may provide information which is not obtainable in gas collisions. The high density of the target may in some cases open up opportunities for studying new collision phenomena, of which a recent example is the possibility of having collision processes in which the incident ion has one or more inner-shell vacancies, produced in a preceding violent collision.[8,9] Such correlated double-collision processes are only probable if the target density is sufficiently high to make it likely for two violent collisions to take place within the very short time interval, corresponding to the lifetime of an inner-shell vacancy, which is typically 10^{-17}–10^{-14} sec.[10]

The present paper is devoted to an analysis of the solid effects. An integral equation describing the thick-target x-ray yields, including contributions from recoil collisions, in terms of excitation cross sections and slowing-down parameters, is established. For low-energy projectiles, where absorption of x rays in the target is negligible, this equation reduces to the integral equation which was established in Ref. 7. The influence of the charge and excitation state of the projectile ions on the probability for producing inner-shell vacancies is discussed. To support and substantiate the analysis of the solid effects, a series of experimental x-ray measurements in ion-solid collisions has been performed. Furthermore, x-ray data which have been published by various authors are reexamined.

II. SOLID EFFECTS

The MO model, which is based on a simplified picture of the colliding heavy-ion–atom system, is known to be in good accord with available experimental data on gas collisions.[1,3] Before discussing the specific solid effects encountered in ion-solid collisions, it is appropriate to summarize some of the qualitative predictions, which can be made from the MO model.

(i) An inner-shell vacancy can only be produced if there exists a vacancy in a higher MO to which the inner-shell electron may go. For example in Na^{++}-Ne collisions the precollision $2p$ vacancy in sodium may become a $2p\pi$ vacancy to which a $2p\sigma$ electron, i.e., a neon K electron, may be transferred as a result of a $2p\sigma$-$2p\pi$ rotational coupling, whereas in Na^{+}-Ne collisions no such $2p\pi$ vacancies are available and the probability for a K ionization is very small.[5] This type of charge-state effect, where, according to the correlation diagram, the ionization of one of the particles produces a MO vacancy to which an inner-shell electron may go during the collision, will be called the *direct* charge-state effect. It is seen to have the effect of opening up an originally closed exit channel for inner-shell ionization.

(ii) An inner-shell vacancy is preferentially produced in the collision partner whose inner-shell electrons have the smallest binding energy. For partners whose atomic numbers do not differ much, this implies that the vacancy is produced in the collision partner with the lower atomic number, e.g., in a S^{+}-Ar collision, the $L_{2,3}$ vacancy is produced in the sulphur ion.[11]

(iii) MO correlation diagrams are ordinarily constructed for neutral atom-atom systems.[3] In the limit of separated atoms ($R \to \infty$), the energy levels for ionized systems may deviate appreciably from those for neutral systems, such that

ionized systems require their own specific diagrams.[12] The order of atomic orbitals may be changed if the ionization of one of the partners causes a substantial change in the binding energies of its outer electrons. As discussed by Barat and Lichten,[3] the state of the outer shells should have little effect on the dynamic couplings causing inner-shell excitations. On the other hand, the availability of vacancies in the MO that serves as exit channel for the inner-shell excitation in question may depend strongly on the state of the outer shells. Since the probability for producing an inner-shell excitation is largely determined by the number of vacancies in the exit channel, it is expected that swapping among the outer-shell orbitals, caused by a high charge state of the incident projectile, may influence that probability. This *indirect* charge-state effect will be most significant when the exit channel is closed for the neutral system. Let us illustrate the effect by an example. In Ne-Mg collisions the exit channel for neon K ionization is closed, see Fig. 1. If the neon atom is initially doubly ionized, the binding energy[13] of the $2p$ orbital of Ne^{++} is larger than the binding energy of the $2p$ orbital of magnesium. A swapping of neon and magnesium $2p$ orbitals results, such that during the collision a neon $2p$ vacancy may become a $2p\pi$ vacancy and thereby make a Ne K excitation possible. This effect may qualitatively be accounted for if correlation diagrams for ionized systems are constructed from the corresponding diagrams for neutral systems by changing the energy levels in the separated limit to their correct position without any change in the correlations. When levels are swapped by this rearrangement, new crossings are introduced and an electron may be transferred from one MO to another at one of these crossings during the collision. The strength of the couplings at these crossings then determines the significance of this indirect charge-state effect.

Let us now consider the x-ray generation in thick targets by heavy-ion bombardment. Although such experiments may be used to trace very small quantities of unknown materials[1] or to locate impurities in crystal lattices,[1] these studies will often have the purpose of providing yield data, which can be converted into specific cross sections. However, such a data reduction is hampered by several solid effects. These effects will be discussed in the following in greater detail.

A. Dependence on Charge and Excitation State

Owing to relatively large cross sections for changes in the projectile charge or excitation state, incident-keV ions will, after having traversed a few atomic layers of the solid, usually attain an equilibrium-charge and excitation-state distribution.[14] Accordingly, the initial charge state of the incident ions is generally not an important parameter in determining the x-ray yield in ion-solid experiments at beam energies well above the threshold energy for the exciation process in question. Since, however, the state of the collision partners prior to the collision event in some cases has a large effect on the probability for an inner-shell ionization, e.g., in opening a closed exit channel, the actual distribution of charge and excitation states of the projectiles during the slowing down in the solid may be an important quantity in determining the x-ray emission yield. Let us for the sake of argument assume that it is possible to divide projectile states into two groups, such that the exit channel for the excitation process in question is closed for projectile states in the first group but open for projectile states in the other. At a given residual projectile energy in the solid, an equilibrium fraction of projectile states belongs to the second group. Only this fraction of the ions will contribute to the production of inner-shell vacancies.

Let us illustrate the charge-state effects in connection with ion-solid collisions by examples. In an Al^{+}-Al single collision there is no Al $2p$ vacancies prior to the collision and hence no $2p\pi$ vacancies are produced during the collision; therefore a K electron cannot be transferred to a $2p\pi$ MO. However, as a result of the ion-solid interaction, a distribution of projectile states is reached of which a fraction allows for an open exit channel for Al K excitations. For example, $2p$ vacancies exist for ions such as Al^{++++} and $Al^{0}(2p^{-1})$. Consequently, the probability for producing an Al K vacancy is appreciable for this fraction of the distribution. This example has illustrated the direct charge-state effect. In Ne^{+}-Al collisions the exit channel for producing neon K vacancies is closed, see Fig. 1. As a result of the ion-solid interactions, the Ne ions achieve a charge-state distribution of which a fraction may have a charge state of 3 or more. For these ions the binding energy[13] of the remaining $2p$ electrons is higher than the corresponding value for neutral aluminium and the indirect charge-state effect may come into play. For such highly charged Ne ions, the exit channel for producing Ne K vacancies is therefore open and the Ne K x-ray production cross section is high.

B. Contributions from Recoil Collisions

During the slowing-down process the incident ions undergo several violent collisions with the

target atoms, thereby producing energetic recoil atoms. The recoils, in turn, may collide with other target atoms and produce inner-shell excitations. In most previous experimental studies of target x rays, contributions from recoil collisions have been neglected. As shown by Taulbjerg and Sigmund,[7] this simplification of the data treatment is often not justified. For some ion-target combinations, recoils may even account for almost all the emitted x rays.

The energy spectrum of the recoils is peaked at low energies. It is therefore expected that the recoil effect is of minor importance in those cases where the incident ions very efficiently produce inner-shell excitations in direct encounters with the target atoms. If, on the other hand, the direct production of inner-shell vacancies is inhibited by a closed exit channel, then the relative importance of the recoils in producing inner-shell vacancies may become substantial. A relevant example is P-C collisions. As may be seen from the MO correlation diagram, the direct production of carbon K vacancies is forbidden by a closed exit channel. The $2p\pi$ MO is filled, so that no $2p\sigma$ (or carbon K) electrons can be transferred to the $2p\pi$ MO. The indirect process, where energetic recoils perform collisions with other target atoms, has no such limitations. In accordance with the MO model, a C-C collision is efficient in producing carbon K vacancies. There are several other examples where the recoils play a major role in generating target x rays.

It can generally be concluded that recoils contribute significantly to the generation of target x rays when direct collisions have a low probability of producing inner-shell vacancies or when the incident ions are substantially heavier than the target atoms. In the latter case the velocity of a recoil atom may exceed the velocity of the incident projectiles and, furthermore, the nuclear stopping dominates over the electron stopping, which is favorable for the creation of energetic recoils.

III. CONNECTION BETWEEN X-RAY PRODUCTION CROSS SECTIONS AND THICK-TARGET YIELDS

During the slowing down of incident ions in a thick solid target, the ions undergo multiple collisions with the target atoms and the observed x-ray yield represents an integration over these collisions. To extract information on the single-collision ionization cross section, this integration has to be unfolded. Cumulative effects in ion-solid interactions are generally described by integral equations. Radiation damage and ion-range theory offer several examples of such descriptions and their numerical solutions.[15-17] The equation governing the yield I of a characteristic x ray involves the corresponding x-ray production cross section σ_x as a source term. As will be discussed in the following, approximations are needed to evaluate σ_x from yield data. Since a detailed derivation of analogous integral equations has been discussed elsewhere,[15,17] we shall not here derive the equation but merely state the results.

The x-ray production cross section in an ion-atom collision is a function of energy E and charge and excitation state of the projectile, i.e., $\sigma_x = \sigma_x(E, Z^*)$, where Z^* characterizes the precollisional state of the projectile. Let us first discuss what information ion-solid x-ray yields can give about $\sigma_x(E, Z^*)$ and its dependence of the precollisional charge state Z^*. To simplify the analysis but without loss of generality in the conclusions, it is assumed that (i) the projectile is stopped completely in the target, (ii) slowing down is caused by random collisions, (iii) the absorption of x rays in the target is negligible, and (iv) recoil collisions do not contribute to the x-ray yield. By the method described in Ref. 15 the yield I and σ_x are then connected by the following equation:

$$\sigma_x(E, Z^*) = \sum_{\hat{Z}^*} \int d\hat{E}\, K(E, Z^*; \hat{E}, \hat{Z}^*) \times [I(E, Z^*) - I(\hat{E}, \hat{Z}^*)], \qquad (1)$$

where K is the differential cross section for a collision which changes the initial projectile energy and charge state (E, Z^*) into $(\hat{E}, \hat{Z}^*)$. To obtain $\sigma_x(E, Z^*)$ from Eq. (1) it is necessary to measure the yield I versus energy and charge and excitation state of incident particles. However, at ion energies considerably higher than the threshold energy for the creation of the x rays in question, most x-ray producing collisions take place after the equilibrium distribution of states has been established, and hence the x-ray yield is almost independent of the initial state of the incident projectiles. In fact, charge-state effects have not been reported in thick-target x-ray yields. This does of course not mean that σ_x is independent of Z^*, but rather that this dependence cannot be derived from thick-target experiments. It is then natural to let the experimental yield function $I(E)$ be a function of energy only. The source term in the equation governing $I(E)$ must then also be a function of energy only, i.e., $\bar{\sigma}_x(E)$. The equation connecting I and $\bar{\sigma}_x$ is

$$\bar{\sigma}_x(E) = \int d\hat{E}\, K(E, \hat{E})[I(E) - I(\hat{E})], \qquad (2)$$

where $K(E, \hat{E})$ is the cross section for a collision where the initial and final projectile energies are

E and $\hat{E}$, respectively. Obviously, the source term $\bar{\sigma}_x(E)$ in this integral equation has to account correctly for the x-ray production in all collisions that take place during the slowing down of a projectile, and since most x-ray producing collisions take place after an equilibrium distribution of projectile states has been achieved, $\bar{\sigma}_x(E)$ represents an average of $\sigma_x(E, Z^*)$ over this distribution.[7] The interpretation of $\bar{\sigma}_x$, derived from experimental yields by means of Eq. (2), as a production cross section averaged over the equilibrium distribution of projectile states is correct only to the extent that the observed yields are independent of the initial state of the projectiles.

Having discussed the meaning of the source term $\bar{\sigma}_x$, we will next turn to the general case where absorption of x rays in the target and recoil collisions may no longer be neglected. The yield will now depend on both the energy and $\eta = \cos\theta$, where θ is the angle between the beam direction and the surface normal. Neglecting terms due to surface effects, the yield function $I(E, \eta)$ is connected to the average production cross section $\bar{\sigma}_x(E)$ by the equation

$$\bar{\sigma}_x(E) + \int d\sigma I_R(T, \eta'') = \frac{\mu\eta}{N\cos\varphi} I(E, \eta) + S_e(E) \frac{dI(E, \eta)}{dE} + \int d\sigma [I(E, \eta) - I(E - T, \eta')], \tag{3}$$

where $d\sigma = d\sigma(E, \eta; E - T, \eta'; T, \eta'')$ is the differential scattering cross section, T being the energy transfer to the recoil atom in a collision, η' and η'' are the cosines of the angles between the surface normal and the vector velocities of the scattered particle and the recoil, respectively. I_R is the yield produced by a recoil atom, i.e., the thick-target yield in the case where the projectiles and the target atoms are of the same element. S_e is the electronic-stopping cross section of the projectile, μ is the x-ray absorption coefficient of the target, N is the density of target atoms, and φ is the angle between the surface normal and the direction of the x-ray detector. In deriving the above equation it is assumed that the slowing down is caused by random collisions and that electronic and nuclear collisions are uncorrelated.[7] In the case of a large mass ratio M_2/M_1 (M_1 is the ion mass, M_2 is the target mass) and low-energy projectiles, surface effects cannot be neglected.[18] Then a general yield equation,[19] which includes ion-backscattering and target-atom sputtering, should be used. This equation is, however, far too complicated to be applicable in the evaluation of experimental data.

It is appropriate to rearrange the terms in Eq. (3). We introduce the nuclear-stopping cross section $S_n = \int d\sigma T$ and the total-stopping cross section $S = S_n + S_e$ and obtain

$$\bar{\sigma}_x(E) + \int d\sigma I_R(T, \eta'') = S(E) \frac{dI(E, \eta)}{dE} - \int d\sigma [I(E - T, \eta) + T \frac{dI(E, \eta)}{dE} - I(E, \eta)] + \frac{\mu\eta}{N\cos\varphi} I(E, \eta) - \int d\sigma [I(E - T, \eta') - I(E - T, \eta)]. \tag{4}$$

At high energies, light-incident particles such as protons and α particles are to a good approximation subject to a continuous slowing down along straight-line trajectories. If, further, the recoil contribution is neglected, the three integrals in Eq. (4) vanish and we obtain the equation also known as Merzbacher's formula[20] for the x-ray production cross section

$$\bar{\sigma}_x(E) = S(E) \frac{dI(E)}{dE} + \frac{\mu\eta}{N\cos\varphi} I(E). \tag{5}$$

Usually, the variation of the x-ray yield versus the angular coordinate is not measured. Then the recoil term

$$\sigma_R(E, \eta) = \int d\sigma I_R(T, \eta'') \tag{6}$$

can only be evaluated if I_R is independent of η''. This is, to a good approximation, the case when the penetration depth in the target of a recoil atom with maximum energy is much smaller than the characteristic length for x-ray absorption μ^{-1}, i.e.,

$$\mu R_p(T_m) \ll 1, \tag{7}$$

where $R_p(T_m)$ is the penetration depth of a target atom with energy $T_m = \gamma E$, $\gamma = 4M_1M_2/(M_1 + M_2)^2$. When this condition is fulfilled, we have

$$\sigma_R(E, \eta) = \int_{\eta'' \geq 0} d\sigma I_R(T, \eta). \tag{8}$$

The integration over angular coordinates may now easily be performed and we obtain

$$\sigma_R(E, \eta) = \int d\sigma(E, T) f_\eta(T/\gamma E) I_R(T, \eta), \tag{9a}$$

where $d\sigma(E, T)$ is the differential cross section for a collision with energy transfer T, and the function f_η is given by

$$f_\eta(x)=\begin{cases}1 & \text{if } x\geq 1-\eta^2,\\ \frac{1}{\pi}\arccos\left[-\frac{\eta}{(1-\eta^2)^{1/2}}\left(\frac{x}{1-x}\right)^{1/2}\right] & \text{if } x<1-\eta^2.\end{cases} \tag{9b}$$

In Ref. 7 the function f_η was set equal to unity in the recoil integral. This approximation is exact only if the target is placed perpendicular to the beam ($\eta=1$) or if the maximum energy transfer $T_m=\gamma E$ is close to the threshold energy in the yield function I_R. Since, however, yield functions generally increase very steeply with increasing energy, the significance of f_η, being different from unity in the integral in Eq. (9a), is usually small.

The variation in the yield versus the angular coordinate is mainly due to absorption of x rays in the target. The last two terms in Eq. (4) may therefore both be interpreted as absorption terms. Then, the last term on the right-hand side of Eq. (4) has apparently the effect of correcting the other absorption term for nonstraight ion trajectories. It is easily seen that this correction is negative. Since the sum of the absorption terms obviously is positive, the magnitude of the correction term is smaller than the leading term. For ion-target combinations where the majority of paths in the ion path distribution is confined within a narrow cone around the initial beam direction, the correction due to nonstraight ion trajectories is small. Only in the case of low-ion energy and large-mass ratio, i.e., $M_1 \ll M_2$, the transverse width of the ion-path distribution may become comparable to the average projected range of the ion.[17] When such cases are excluded, the correction term will be negligible compared to the other term in Eq. (4) if the leading absorption term is small, i.e., if

$$\mu R_p(E)\eta/\cos\varphi \lesssim 1, \tag{10}$$

where R_p is the penetration depth of a projectile of energy E. If, further, condition (7) is fulfilled, Eq. (4) depends only parametrically on the angular coordinates and the equation reduces to

$$\Sigma_x(E)=S(E)\frac{dI(E)}{dE} - \int d\sigma(E,T)\left(I(E-T)+T\frac{dI(E)}{dE}-I(E)\right) + \frac{\mu\eta}{N\cos\varphi}I(E), \tag{11}$$

where the generalized x-ray production cross section is defined by

$$\Sigma_x(E)=\bar{\sigma}_x(E)+\sigma_R(E) \tag{12}$$

and $\sigma_R(E)$ is given by Eq. (9). Except for the absorption term and the correction in the recoil term which was discussed above, Eq. (11) is identical with the yield equation given in Ref. 7. If the recoil contribution σ_R and the integral term on the right-hand side of Eq. (11) are neglected, the equation reduces to Eq. (5), the Merzbacher formula.

IV. EXPERIMENT AND DATA EVALUATION

In order to support the discussion of solid effects in connection with the predictions of the MO model, measurements on thick targets of x-ray yields from various ion-solid interactions have been performed (cf. Table I). We have been particularly interested in studying the exit-channel effect and since this effect is most pronounced for K shell excitations, the experimental studies have been confined to K x rays. Actually, we have chosen ion-target combinations in such a way that according to the MO model, the exit channel for the excitation process in question is closed for a single

TABLE I. Parameters P, U, and I_0 giving good fits of Eq. (13) to experimental $I(E)$ curves. Mass-absorption coefficients (μ/ρ) are obtained from Ref. 21. $R(E)=\int_0^E[NS(E)]^{-1}dE$ is the average path length of an ion with energy E.

Projectile	Target	Measured x ray	Projectile energy range (keV)	P	U (keV)	I_0	$\frac{\mu}{\rho}$ (cm^2/g)	μR (E_{max})
Ar	Al	Al(K)	160–450	4.91	70	1.95×10^{-8}	400	0.052
Al	Al	Al(K)	100–200	3.99	70	7.63×10^{-6}	400	
Al	Al	Al(K)	180–500	1.84	130	2.69×10^{-4}	400	0.087
N	Al	Al(K)	200–500	2.85	80	1.11×10^{-8}	400	0.12
Ne	Mg	Ne(K)	80–250	2.54	50	5.72×10^{-6}	1390	
Ne	Mg	Ne(K)	200–500	1.63	105	1.12×10^{-4}	1390	0.38
Ne	Al	Ne(K)	125–500	2.13	65	1.04×10^{-5}	1990	0.47
Ne	Si	Ne(K)	150–500	2.27	85	7.91×10^{-6}	2400	0.57
Ne	P	Ne(K)	250–500	2.47	90	2.57×10^{-6}	2990	0.75

collision between a neutral projectile and a target atom.

The experimental setup consists of a target holder upon which three targets can be mounted simultaneously. The beam current to the target holder is monitored and secondary electron effects are suppressed by an electrostatic shield in front of the target. The angles between the beam and the surface normal θ and between the x-ray proportional detector and the surface normal φ are both 45°, i.e., $\eta = \cos\theta = \cos\varphi$. The detector, which has a 6-μ Mylar window and is floated with methane, can be used with or without an additional 6-μ Mylar absorber foil from the same batch as the window. In this way, detector-efficiency corrections can easily be made and with better accuracy than can be obtained from the knowledge of the absolute thickness and tabulated values of the absorption.

At higher beam energies the uncertainty in absolute yield, which mainly is due to the limited accuracy in the determination of the solid angle and the efficiency of the detector, is estimated to be less than ±20%, whereas the relative accuracy is better than ±5%, limited mainly by the uncertainty in the beam-current integration. At lower energies the uncertainties are increased by statistical errors due to low counting rates and increased detector background contribution which makes it difficult to obtain reliable yields close to the threshold energy for the x-ray production.

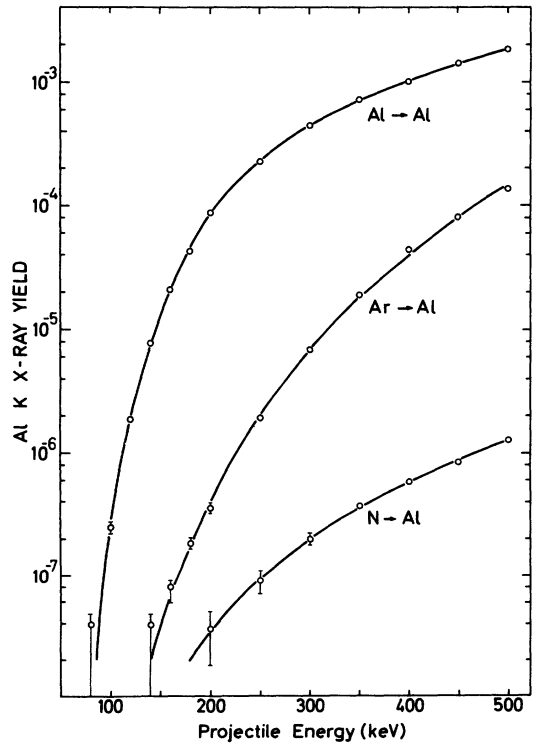

FIG. 2. Aluminium K x-ray yields versus energy of N, Al, and Ar ions incident on thick aluminium targets. Unless indicated, the relative uncertainties are less than ±5%. The uncertainty in absolute scale is estimated to be less than ± 20%. Analytic fits to the data points are shown by solid lines.

To facilitate the evaluation of the cross sections, an expression of the form[7]

$$I(E) = I_0(E/U - 1)^P \tag{13}$$

has been fitted to the experimental data points. Parameters I_0, U, and P, giving good fits, are listed in Table I. The data points scatter randomly around the smooth-fitting curve and their deviations are well accounted for by the relative uncertainties in the data points. As an example, the aluminium K x-ray-yield data and the fitted yield functions are shown in Fig. 2.

The conditions for the applicability of Eqs. (11) and (9) are fulfilled in all cases (cf. Table I). When $d\sigma$ and S_e are known, Σ_x and σ_R can be evaluated by numerical integration without introducing further approximations. Differential elastic-scattering cross sections based on various screened Coulomb interactions are well represented by the expression[22]

$$d\sigma(E, T) = CE^{-m}T^{-1-m} \times [1 + C_1(ET)^{q(1-m)}]^{-1/q} dT, \ \ldots, \ T \leq T_m, \ \ldots, \tag{14}$$

where the maximum energy transfer $T_m = \gamma E$. C and C_1 are constants depending on the ion-target combination only. The parameters m and q are set equal to $\frac{1}{3}$ and $\frac{2}{3}$, respectively, corresponding to an approximate Thomas-Fermi cross section.[17] The following expression for the nuclear-stopping cross section is then obtained:

$$S_n(E) = \frac{9C}{4C_1^{3/2}E}\left[\ln\left(\frac{1 + (1-x)^{1/2}}{1 - (1-x)^{1/2}}\right) - 2(1-x)^{1/2}\right], \tag{15}$$

where $x = x(E) = [1 + C_1(\gamma E^2)^{4/9}]^{-1}$. Since experimental data on the electronic-stopping cross section in the appropriate energy region are not available, the velocity proportional stopping formula

$$S_e(E) = K\sqrt{E}\,, \tag{16}$$

where K depends on the ion-target combination,[16] has been applied.

The experimental results are presented in Figs. 3 and 4. Figure 3 shows Al K x-ray data from aluminium targets. The generalized solid-target x-ray production cross section Σ_x and the recoil contribution σ_R are shown separately. The direct

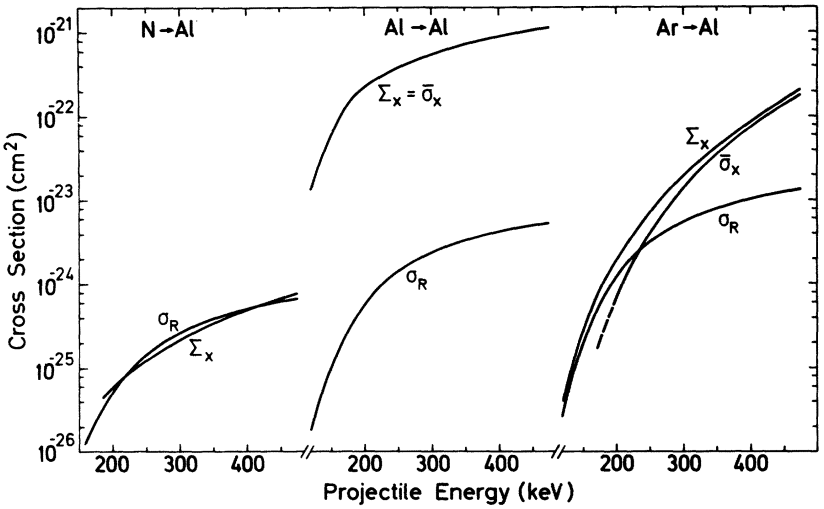

FIG. 3. Aluminium K x-ray production cross sections versus the energy of incident N, Al, and Ar ions. The generalized cross section $\Sigma_x = \bar{\sigma}_x + \sigma_R$ is evaluated according to Eq. (11). The recoil part σ_R is obtained by means of Eqs. (9). $\bar{\sigma}_x$ is the cross section in direct collisions between the incident projectile and a target atom. Within the uncertainties of the experimental data and the analysis, Σ_x equals σ_R in the case of N-Al such that only an upper limit to σ_x may be obtained.

cross section $\bar{\sigma}_x$ is, according to Eq. (12), obtained by subtraction. Figure 4 shows Ne K x-ray data for neon projectiles incident on various solid targets. Since projectile x rays are measured, no contribution from recoil collisions is present. For comparison are also shown data by Saris and Onderdelinden[23] and Tawara *et al.*[24] on Ne^+-Ne and Ne^{++}-Ne. As to the importance of the straggling term, i.e., the integral term in Eq. (11), sizable values—up to 30%—are found at low projectile energies.

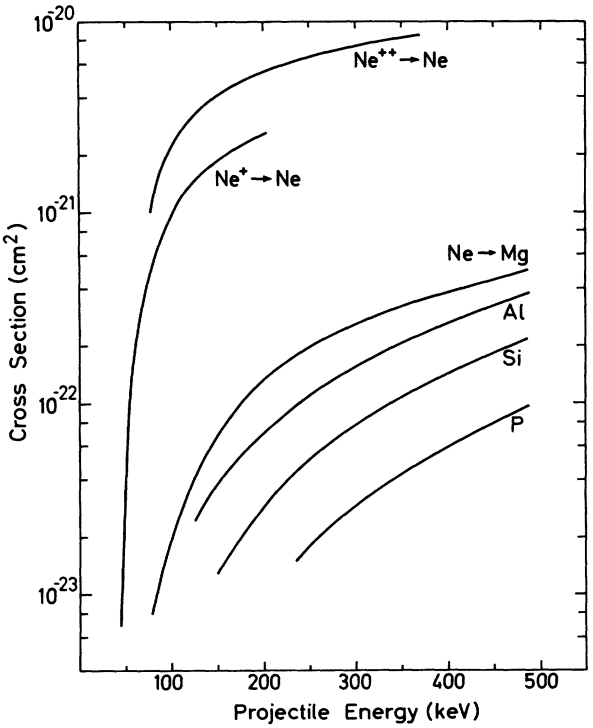

FIG. 4. Neon K x-ray production cross sections versus the energy of neon ions incident on solid targets of the elements Mg, Al, Si, and P. For comparison are also shown the K x-ray production cross sections in Ne^+-Ne and Ne^{++}-Ne collisions obtained by Saris and Onderdelinden (Ref. 23) and Tawara *et al.* (Ref. 24).

V. DISCUSSION

A. Recoil Effect

As expected, the recoil contribution σ_R in relation to the Al K x-ray production in aluminium targets (cf. Fig. 3), increases with the increase of the atomic number of the projectiles. The fraction of Al K x rays, which is produced by recoil collisions, may, however, be large for low-Z projectiles. An example of this is the N-Al case, where collisions undergone by recoil atoms completely dominate the Al K x-ray production. Within the uncertainty of the experimental data and the analysis, σ_R equals the generalized cross section Σ_x and hence the direct x-ray production cross section $\bar{\sigma}_x$ is at least one order of magnitude smaller than Σ_x. The reason for this strong dominance of the recoil effect is seen from the correlation diagram, Fig. 1. The $1s\sigma$ MO, which correlates with the Al 1s level, does not cross any MO and hence the exit channel for an Al K ionization in a direct N-Al collision is closed. In the symmetric collision, Al-Al, it is noted that the recoil contribution as compared to the contribution of direct collisions is small. This is also expected since the Al projectiles have a high kinetic energy, whereas the recoil Al atoms are mainly low-energy particles and therefore less efficient in producing Al K x rays. In the last case, Ar-Al, a strong competition between direct and recoil collisions produced Al K x rays is noted. At ion energies below approximately 235 keV, σ_R is larger than $\bar{\sigma}_x$, and as the energy is further reduced (below 160 keV), σ_R is approximately equal

to Σ_x and, accordingly, the direct-production cross section becomes very small. At energies above 235 keV, the major fraction of produced Al K x rays pertains to direct Ar-Al collisions and the recoil contribution is less important.

B. Charge-State Effects

For all the collisions studied (cf. Figs. 3 and 4) a definite charge-state effect is present. According to the correlation diagram for a neutral atom-atom system, none of these collisions have an open exit channel for producing a K ionization.

Let us first look at the data shown in Fig. 3. Here it is of interest to discuss the production of Al K x rays in Al-Al collisions and in Ar-Al collisions, simultaneously. In both cases projectile $2p$ vacancies are needed to open the exit channels for Al K excitations. As discussed in Sec. II, these vacancies may be obtained as a result of the ion-solid interaction. Accordingly, the probability for an ion at a given energy to have a $2p$ vacancy or—equivalently—the equilibrium fraction of projectiles having such vacancies, is an important parameter. This fraction is determined by the production rate for these $2p$ vacancies and by their decay rate. Argon $2p$ vacancies may, in Ar-Al collisions (cf. Fig. 1), be produced through the $3d\sigma$-$3p\pi$ rotational coupling. The internuclear separations, at which this rotational coupling is efficient, are very small. Argon $2p$ vacancies are therefore only created during violent encounters, whereas Al $2p$ vacancies are expected to be produced in rather soft Al-Al collisions, where the $4f\sigma$ promotion is effective. The production rate of projectile $2p$ vacancies is, consequently, significantly larger for Al projectiles than for Ar projectiles. Though the decay rates are affected by outer-shell ionization and by quenching collisions, an order-of-magnitude estimate may be obtained by comparing the theoretical lifetimes. The lifetime of a $2p$ vacancy in aluminium is an order of magnitude larger than the corresponding lifetime for argon.[10] The fraction of projectiles having $2p$ vacancies is therefore much smaller for Ar than for Al. This is consistent with the observation that $\bar{\sigma}_x$ for argon impacts is much smaller than for aluminium impacts. The fact that argon L vacancies are produced by a rotational coupling, in contrast to the aluminium case where an almost energy-independent $4f\sigma$ promotion mechanism produces the L vacancies, seems to explain why $\bar{\sigma}_x$ for Ar-Al collisions has a steeper energy dependence than $\bar{\sigma}_x$ for Al-Al collisions.

Whereas Fig. 3 illustrates the importance of the direct charge-state effect, Fig. 4 gives examples of the indirect charge state effect. Neon K x rays have been measured for neon ions incident on Mg, Al, Si, and P targets. It is evident that recoil collisions play no role in the production of neon K x rays, such that the generalized cross section Σ_x equals the direct cross section $\bar{\sigma}_x$. Since neon in all cases is the lighter collision partner, the correlation diagram on Fig. 1 predicts that a neon K ionization is only feasible if the target atom has one or more $2p$ vacancies before the collision, which may become $2p\pi$ vacancies as the nuclei approach each other. Clearly, the target atoms are not ionized before the collision and hence a direct charge-state effect cannot explain the substantial neon K ionization cross section observed. However, during the slowing down process the neon projectiles are multiply ionized, such that a fraction of these projectiles may have a sufficiently high charge state to cause a swapping of $2p$ neon levels and $2p$ levels of the target atoms. From values of inner-shell binding energies[13] for ions in various charge states it is estimated that the critical projectile charge Z_c^* for a swapping of the $2p$ levels of neon and target atoms is 2, 3, 4, and 5 for targets of Mg, Al, Si, and P, respectively. For excited neon ions swapping may occur at lower charge states. As was discussed in Sec. II, the swapping of two $2p$ levels results in new crossing, e.g., the $2p\pi$ MO and the $3d\pi$ MO may perform a crossing. Through the action of such crossing, a neon $2p$ vacancy may become a $2p\pi$ vacancy, and the exit channel for the production of neon K x rays has been opened.

The indirect charge-state effect is supported by several qualitative features of the data. First, although no charge-state data exist for the collision system under investigation here, it may be appropriate to use existing data for neon ions passing through a thin carbon foil.[14] For 482-keV Ne ions, the charge-state distribution of the emerging neon ions is Ne^0(5%), Ne^+(27%), Ne^{++}(39%), Ne^{+++}(25%), and Ne^{++++}(4%). It is likely that the charge-state distribution does not depend sensitively on the target element. In addition to this, the average number of L vacancies inside a solid target may be somewhat higher than the measured value of the charge for the emerging ions. From these considerations we may conclude that the equilibrium charge-state distribution is sufficiently wide to cause a swapping of the $2p$ orbitals for an appreciable fraction of the projectile–target-atom collisions.

Secondly, the absolute value of $\bar{\sigma}_x$ decreases with increasing Z_2. This is qualitatively in accordance with a corresponding decrease of the fraction of the projectiles being in a sufficiently high charge state to cause swapping.

Thirdly, the slope of the energy dependence of

$\bar{\sigma}_x$ gets steeper when Z_2 is increased. This is consistent with the fact that (i) the charge-state distribution is shifted towards higher charge states when the ion energy is increased and (ii) the relative gain obtained by this shift in the fraction of projectile states causing swapping becomes higher at higher-Z_2 values.

Finally, for comparison the x-ray production cross sections[23,24] for Ne^+-Ne and Ne^{++}-Ne are shown in Fig. 4. For these collisions, where a direct charge-state effect is known to operate, the x-ray production cross section is an order of magnitude larger than the corresponding cross section for Ne-Mg collisions. The reason for this deviation in the cross section is mainly twofold. First, only a fraction of the neon projectiles in Ne-Mg collisions has a charge and excitation state resulting in swapping of the $2p$ levels. Second, even when the levels are swapped, the probability of transferring a neon $2p$ vacancy into the $2p\pi$ MO may be considerably smaller than the corresponding probability for the Ne^+-Ne case since the new crossing created by the swapping of the $2p$ levels may have a fairly low probability of transferring a $3d\pi$ vacancy into a $2p\pi$ vacancy.

Although there seems to be good evidence for the existence of the indirect charge-state effect, it ought to be pointed out that more conclusive experiments are needed before the effect is firmly founded.

VI. SOLID EFFECTS IN PUBLISHED DATA

It has recently been shown[7] that the production of carbon K-shell excitations by Kr and Xe ions[25] is spuriously high because of recoil effects. This observation eliminates a serious discrepancy[3] between the experimental results and the MO model.

Brandt and Laubert[26] have measured the Al K x-ray production of aluminium targets bombarded with N, O, Ne, and Ar ions. The recoil effect was estimated by these authors[27] to be rather unimportant at high projectile energies. At low and moderate energies, contributions from recoil collisions were not taken into account. Except for the straggling term, the x-ray production cross sections reported by these authors are therefore the generalized cross section Σ_x rather than the direct cross section $\bar{\sigma}_x$. For the cases of O and Ne impacts, Brandt and Laubert measured K-ionization cross sections slightly higher than the one obtained for N-Al. Since the recoil contribution to the x-ray yield is increasing with Z_1 and we know that it dominates for N-Al collisions, we may conclude that recoil contributions will also dominate for the cases of O-Al and Ne-Al. Consequently, the apparent discrepancy between the low-energy data by Brandt and Laubert and the MO model is eliminated.

Macek and co-workers[9] observed Si K x rays when solid silicon was bombarded with 120–260-keV Ar ions and interpreted the results obtained in terms of a projectile double-scattering mechanism. It is likely that the contribution from recoil collisions is appreciable, if not dominating, as found in the same energy region for our data on Al K x rays from aluminium targets bombarded with Ar ions.

Let us finally discuss the data reported by Kavanagh and co-workers[28] on copper L-shell ionization in collisions between Cu and a very wide range of heavy ions and atoms. Using Eq. (5) these authors evaluated the Cu L x-ray production cross section from the solid-target yields both in the case of copper targets and in the case of incident copper ions. The observed oscillations in the production cross section versus the atomic number of the other collision partner at fixed ion velocity were considered as evidence for the so-

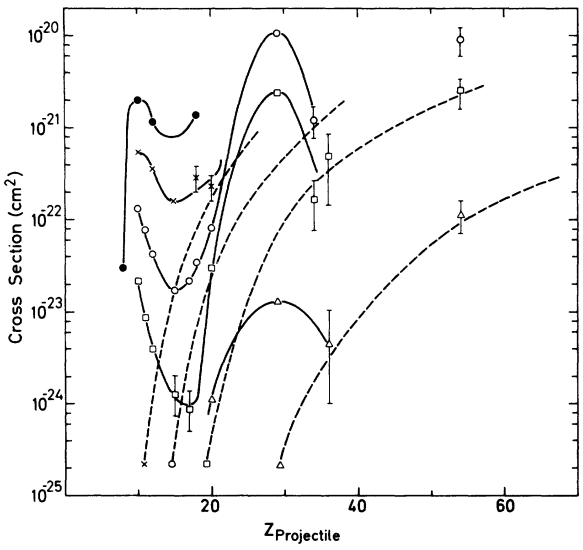

FIG. 5. Cross sections for copper L x-ray production in thick copper targets as a function of the atomic number of the incident ion for different fixed ion velocities: triangles, 1.0 keV/amu; squares, 2.0 keV/amu; open circles, 3.0 keV/amu; crosses, 5 keV/amu; filled circles, 10 keV/amu. The cross sections are reevaluated on the basis of the yield data (Ref. 29) obtained by Kavanagh *et al.* (Ref. 28). The solid lines represent the generalized x-ray-production cross section Σ_x. Each dashed line corresponds to one of the solid lines and represents the recoil part σ_R. The direct x-ray-production cross section $\bar{\sigma}_x$ is not plotted since, for Z_1 less than 30, $\bar{\sigma}_x$ is almost equal to Σ_x, and for Z_1 larger than 30, $\bar{\sigma}_x$ is the small difference between almost equal numbers and cannot be determined accurately.

called level-matching effect. The authors further noted a subshell effect in their data. The cross section for xenon ($Z_1 = 54$) on copper appeared to be near a peak value, whereas the corresponding peak for Cu projectiles occurred at $Z_2 = 64$. The original data analysis, however, suffered from two defects: (i) Using Eq. (5), the energy straggling was ignored. This may give a sizable correction to the reported cross section, up to 40% for the heavier incident particles. (ii) In the case of copper as a target, the recoil contribution was ignored. Based on the original yield data,[29] the cross sections have been reevaluated using Eq. (11). The cross sections for copper as target are presented in Fig. 5. To illustrate the importance of the recoil contribution both the results for Σ_x, the generalized cross section and σ_R, the recoil contribution, have been plotted. The cross section in direct projectile-target-atom collisions $\bar{\sigma}_x$, may then be obtained by subtraction, i.e., $\bar{\sigma}_x = \Sigma_x - \sigma_R$. From Fig. 5 it is seen that in the cases of Se, Kr, and Xe projectiles the recoil contribution falls within the error bars on Σ_x and accordingly $\bar{\sigma}_x$ is small. This result is particularly interesting as it removes the apparent subshell effect, which was observed by Kavanagh and coworkers.

ACKNOWLEDGMENTS

We would like to thank Dr. T. M. Kavanagh for supplying us with the copper x-ray-yield data, and Peter Sigmund for many helpful discussions.

[1]Q. C. Kessel and B. Fastrup, in *Case Studies in Atomic Physics*, edited by E. W. McDaniel and M. R. C. McDowell (North-Holland, Amsterdam, 1973), Vol. III.
[2]U. Fano and W. Lichten, Phys. Rev. Lett. 14, 627 (1965).
[3]M. Barat and W. Lichten, Phys. Rev. A 6, 211 (1972).
[4]F. T. Smith, Phys. Rev. 179, 111 (1969).
[5]B. Fastrup, G. Hermann, and Q. C. Kessel, Phys. Rev. Lett. 27, 771 (1971).
[6]M. P. McCaughey, E. J. Knystautas, H. C. Hayden, and E. Everhart, Phys. Rev. Lett. 21, 65 (1968).
[7]K. Taulbjerg and P. Sigmund, Phys. Rev. A 5, 1285 (1972).
[8]F. W. Saris, W. F. van der Weg, H. Tawara, and R. Laubert, Phys. Rev. Lett. 28, 717 (1972).
[9]J. Macek, J. A. Cairns, and J. S. Briggs, Phys. Rev. Lett. 28, 1298 (1972).
[10]E. J. McGuire, Phys. Rev. A 3, 587 (1971).
[11]B. Fastrup, G. Hermann, and K. J. Smith, Phys. Rev. A 3, 1591 (1971).
[12]R. C. Der, R. J. Fortner, T. M. Kavanagh, and J. D. Garcia, Phys. Rev. Lett. 27, 1631 (1971).
[13]W. Lotz, J. Opt. Soc. Am. 58, 915 (1968); J. Opt. Soc. Am. 60, 206 (1970).
[14]P. Hvelplund, E. Laegsgaard, J. Ø. Olesen, and E. H. Pedersen, Nucl. Instrum. Methods 90, 315 (1970).
[15]J. Lindhard, V. Nielsen, M. Scharff, and P. V. Thomsen, Mat. Fys. Medd. Dan. Vid. Selsk. 33, No. 10 (1963).
[16]J. Lindhard, M. Scharff, and H. E. Schiøtt, K. Dan. Vidensk. Selsk. Mat. Fys. Medd. 33, No. 14 (1963).
[17]K. B. Winterbon, P. Sigmund, and J. B. Sanders, K. Dan. Vidensk. Selsk. Mat. Fys. Medd. 37, No. 14 (1970).
[18]J. Bøttiger, J. A. Davies, P. Sigmund, and K. B. Winterbon, Radiat. Eff. 11, 69 (1971).
[19]P. Sigmund and K. Taulbjerg (unpublished).
[20]E. Merzbacher and H. W. Lewis, in *Encyclopaedia of Physics*, edited by S. Flügge (Springer-Verlag, Berlin, 1958), Vol. 34, p. 166.
[21]B. L. Henke, R. L. Elgin, R. E. Lent, and R. B. Ledingham, Norelco Rep. 25, 112 (1967).
[22]K. B. Winterbon, Radiat. Eff. 13, 215 (1972).
[23]F. W. Saris and D. Onderdelinden, Physica (Utr.) 49, 441 (1970).
[24]H. Tawara, C. Forster, and F. J. de Heer, Phys. Lett. A 43, 266 (1973).
[25]R. C. Der, R. J. Fortner, T. M. Kavanagh, and J. M. Khan, Phys. Rev. A 4, 556 (1971).
[26]W. Brandt and R. Laubert, Phys. Rev. Lett. 24, 1037 (1970).
[27]W. Brandt and R. Laubert, Phys. Lett. A 43, 53 (1973).
[28]T. M. Kavanagh, M. E. Cunningham, R. C. Der, R. J. Fortner, J. M. Khan, E. J. Zaharis, and J. D. Garcia, Phys. Rev. Lett. 25, 1473 (1970).
[29]T. M. Kavanagh (private communication).